J. Fluid Mech. (1989), vol. 208, pp. 575–593
Printed in Great Britain

Dendritic growth of an elliptical paraboloid with forced convection in the melt

By RAMAGOPAL ANANTH AND WILLIAM N. GILL†
Department of Chemical Engineering, Rensselaer Polytechnic Institute, Troy, NY 12180-3590, USA

(Received 16 May 1988 and in revised form 26 April 1989)

All experimental observations of the growth of fully developed dendritic ice crystals indicate that the shape of the tip region is an elliptical paraboloid. Therefore, moving-boundary solutions of the three-dimensional Navier–Stokes and energy equations are obtained here for the shape-preserving growth of isothermal elliptical paraboloids by using the Oseen approximation which is valid for the low-Reynolds-number viscous flows which prevail in dendritic growth. Explicit expressions for the flow and the temperature fields are derived in a simple way using Ivantsov's method. It is shown that the growth Péclet number, P_G, is a function of the aspect ratio A, the Stefan number St, the Reynolds number Re, and the Prandtl number Pr. As the Reynolds number increases P_G becomes linear in St, less dependent on A and ultimately varies roughly as $Re^{\frac{1}{2}}$.

A comparison between the exact solutions given here and the experiments of Kallungal (1974) indicate that A decreases as Re increases. This result agrees qualitatively with the experiments of Kallungal (1974) and Chang (1985). The differences between theory and experiments for $Re > 10^{-3}$ may be due to attachment kinetic resistance to growth along the c-axis and capillary effects at the tip which make ice dendrites non-isothermal and create conduction in the solid phase. However, more accurate simultaneous measurements of R_1 and R_2 are needed to determine definitively the mechanisms responsible for these deviations between theory and experiment.

1. Introduction

Dendritic growth is inherently a three-dimensional nonlinear phenomenon which is markedly influenced by the shape (aspect ratio) of the moving interface, especially in the neighbourhood of the leading tip. Two-dimensional representations may underpredict the growth rate of dendrites dramatically, especially at small values of the undercooling ΔT, or Stefan number St. The rate of growth is driven by the transfer of latent heat from the solid–liquid interface which sees a three-dimensional subcooled melt, and the interface (as in the case of ice–water for example) often is not axisymmetric. Because of its fundamental importance, the effect of shape on the growth rate of dendrites in the presence of flow is the subject of this study.

Ivantsov (1947) showed that in the absence of convection, an isothermal paraboloid of revolution grows steadily in a shape-preserving manner. Ananth & Gill (1984) recast Ivantsov's method into a similarity approach and applied it to a two-phase conduction problem. Horvay & Cahn (1961) extended Ivantsov's solution to an elliptical paraboloid and showed that the shape, characterized by the aspect ratio,

† Author to whom correspondence should be addressed.

A, has a large effect on the growth rate. In this work, we shall generalize the results of Horvay & Cahn to include convection by applying the similarity approach to obtain self-consistent moving-boundary solutions of the Navier–Stokes and energy equations in which the Navier–Stokes equations are well approximated by using the Oseen viscous flow equations at low Reynolds numbers Re. We shall show that the effect of shape on the growth of the dendrite tip is very significant, but for a given value of the Stefan number this effect becomes less pronounced as the Reynolds number is increased.

Lagerstrom & Cole (1955) and Lagerstrom (1964) have considered, at low Reynolds numbers, the use of the Oseen equations as uniformly valid approximations of the Navier–Stokes equations. They conclude that the Oseen approximation is appropriate for three-dimensional semi-infinite bodies, i.e. elliptical paraboloids, if the body shrinks to a line and therefore has no 'arresting power' as the Reynolds number goes to zero. Clearly, the elliptical paraboloid shrinks to a line parallel to the flow for $Re \to 0$, A fixed, where the low-Re limit occurs because the lengthscale shrinks to zero. This general statement of Lagerstrom and Cole has been verified numerically by Davis & Werle (1972) who showed that the numerical solution of the Navier–Stokes equation agrees with the Oseen solution over the entire surface of the body for $Re \leqslant 0.05$ and $A = 1$.

Furthermore, for the two-dimensional parabolic cylinder, the Oseen solution is not appropriate because the body shrinks to a semi-infinite plane which does have 'arresting power' and disturbs the flow at infinity. In this case Davis (1972) found that the Oseen equations do not give satisfactory results as $Re \to 0$.

It also is significant that at low Reynolds numbers the Stokes' solution, which applies near the body, is contained in the Oseen approximation. We show this explicitly in Appendix B, and it is noted on page 89 in Lagerstrom's (1964) paper. The solution of Stokes does not satisfy the far-field boundary condition due to the Stokes paradox. The arbitrary constant which appears in this solution is evaluated by matching with the Oseen solution up to order Re'^2.

Several forced convection theories have been reported in the literature for stationary parabolic cylinders or paraboloids of revolution. Fernandez & Barduhn (1967) made the first attempt to predict the growth rate of ice by neglecting the moving boundary and assuming that ice dendrites are parabolic cylinders from which the rate of heat transfer can be determined by making boundary-layer assumptions. Simpson, Beggs & Deans (1975) proposed a creeping-flow model by employing the linearized form of the numerical solutions given by Davis (1972), and Dennis & Walsh (1971). Huang (1975) made two-dimensional thermal convection calculations for a stationary parabolic cylinder using boundary-layer theory. Cantor & Vogel (1977), and Doherty, Cantor & Fairs (1978) assumed that a stagnant film exists near the solid–liquid interface of a paraboloid of revolution and they estimated the film thickness by using forced-convection boundary-layer results which they developed for flow over a flat plate. None of these theories represents adequately the three-dimensional nature of this phenomenon. They all neglect the inherent effect of a moving interface and make boundary-layer assumptions that underestimate the effect of shape on the rate of heat transfer from dendrite tips which may have strong curvature because of their very small dimensions.

Dash & Gill (1984) showed that the Oseen viscous flow approximation, instead of the boundary-layer assumptions, leads to exact forced-convection solutions for parabolic cylinders and paraboloids of revolution. Gill, Ananth & Tirmizi (1987) and Ananth & Gill (1988*a*) generalized the Dash & Gill solutions to include moving

boundaries and showed quantitatively that the movement of the interface creates an apparent convection effect which is increasingly important as the subcooling increases and as the velocity of the melt decreases.

Ananth & Gill (1988*a*, *b*) developed three-dimensional moving-boundary solutions for the growth of axisymmetric dendrites, such as succinonitrile, in the presence of both forced (1988*a*) and thermal (1988*b*) convection. Their results are in good agreement with the experimental data of Huang & Glicksman (1981) on succinonitrile. In contrast to succinonitrile, the tips of ice dendrites have the shape of an elliptical paraboloid which is not axisymmetric. Because all of the existing theories, which include convection, assume that the dendrite is either a paraboloid of revolution or a parabolic cylinder, they fail to predict the growth rate accurately, as shown by Kind, Gill & Ananth (1987). Therefore, we shall study the effects of the moving boundary, the aspect ratio, and forced convection on the growth of the dendrites and compare our analysis with the experimental data on the growth of ice dendrites along the A-axis in order to gain insight into the factors that govern this interesting phenomenon.

Several kinds of experiments have been described in the literature on the free growth of dendritic ice crystals. In all of the experiments where the shape was observed, the tip region was reported to be very close to an elliptical paraboloid. In the experiments performed by Fujioka (1978), Huang & Barduhn (1985) and Tirmizi & Gill (1987) thermal (natural) convection played a significant role. Those by Kallungal & Barduhn (1977), Simpson *et al.* (1975), and Chang & Gill (1987) were dominated by forced convection. In the thermal-convection experiments crystals grow from a capillary tube into a melt which is quiescent except for the flow generated by gravity acting on a density distribution, which is created by the temperature gradients that result when the melt absorbs the heat of fusion, L, of the liquid–solid transformation. One typically encounters velocities of order 10^{-2} cm/s in thermal-convection experiments with ice. In the forced-convection experiments the flow of the subcooled melt is created and controlled by means external to the growth process itself, such as an elevated tank from which flow is throttled under a significant head, and flow velocities up to 70 cm/s have been reported by Kallungal & Barduhn (1977) in which case thermal convection is rendered completely negligible. The non-symmetric shape and the small size of R_1, which is on the order of a few microns, imply that accurate measurements are much more difficult to make in the ice experiments than in the case of succinonitrile, where the tip radius is significantly larger (20 μm). The quantities which should be measured as functions of the subcooling, $\Delta T = T_m - T_\infty$, and the flow rate of the melt, U_∞, in order to compare theory and experiments, are the A-axis growth velocity of the leading tip, V_G, and the tip radii R_1 and R_2. However, to date experimental difficulties have precluded the simultaneous measurement of R_1 and R_2. Therefore, it is necessary to combine the data of Kallungal & Barduhn on R_1 with the values of Chang & Gill for R_2 in order to compare the experiments with our theory which relates the aspect ratio, $A = R_2/R_1$, to P_G, St, Pr, and Re. The experimental data that we have used are for $5 \times 10^{-3} < U_\infty < 70$ cm/s and $0.1 < \Delta T < 1$ K, and can be summarized as follows:

$$V_G = 0.0365\, U_\infty^{\frac{1}{2}}\, \Delta T^{\frac{3}{2}} \text{ cm/s} \qquad \text{(Kallungal 1974)},$$

$$R_1 = 6 \times 10^{-5}/\Delta T \text{ cm} \qquad \text{(Kallungal 1974)},$$

$$R_2 = 1.54 \times 10^{-3}\, U_\infty^{-0.23}\, \Delta T^{-0.9} \text{ cm} \qquad \text{(Chang 1985)}.$$

The analysis presented here and our previous ones provide an infinite set of

solutions from which nature selects one for a given set of experimental conditions for ΔT and U_∞. The ultimate theoretical problem is to predict how fully developed ice dendrites select a particular V_G, R_1 and R_2 for a particular ΔT and U_∞ and it should include the effects of anisotropic interface kinetics and capillarity. To our knowledge this problem has not yet been addressed. We do not consider it here and there are several aspects to the process of selection which seem to be unresolved, as pointed out very recently by Xu (1988).

Our purpose is to provide a new self-consistent base-state solution of the transport equations for the growth of an elliptical paraboloidal interface, the shape of which is known to approximate closely the tip of an ice dendrite, to show how the parameters interact and affect P_G, and to determine the extent to which our moving-boundary solutions to the Oseen and energy equations in the form $P_G = f(A, St, Re, Pr)$ are consistent with the experiments of Kallungal and Chang whose data indicate that the aspect ratio of the tip of ice dendrites decreases as the Reynolds number increases. As explained later, only qualitative comparisons between theory and experiments are possible because of the uncertainties in the data reported for R_1 and R_2, and our assumption that the solid–liquid interface is isothermal.

2. Analysis

To fix ideas, consider the growth of a crystal from a melt which flows uniformly along the direction of the x-axis at a constant velocity U_∞, as shown in figure 1. The x-axis and z-axis in figure 1 correspond to the A-axis and C-axis of the ice crystal respectively. The melt is assumed to be infinite in extent, which implies that the growth of the dendrites is unencumbered by external surfaces. The pressure drop ΔP is created owing to the presence of the crystal. The transfer of the latent heat of fusion from the moving interface to the melt is driven by the difference in temperature between the solid surface, which is assumed to be at the normal melting point T_m, and the bulk of the subcooled melt, which is T_∞. The density of the solid and liquid are equal, and the governing equations for any shape of the interface in fixed, rectilinear coordinates t, X, Y, Z, are given by

$$\nabla \cdot \boldsymbol{U} = 0, \tag{1}$$

$$\frac{\partial \boldsymbol{U}}{\partial t} + \boldsymbol{U} \cdot \nabla \boldsymbol{U} = -\frac{1}{\rho} \nabla P + \nu \nabla^2 \boldsymbol{U}, \tag{2}$$

$$\frac{\partial T}{\partial t} + \boldsymbol{U} \cdot \nabla T = \alpha \nabla^2 T. \tag{3}$$

The boundary conditions are

$$U_X = 0, \quad U_Y = 0, \quad U_Z = 0, \quad T = T_m \tag{4}$$

at $\eta = 1$, which is the surface of the body, and

$$U_X = U_\infty, \quad U_Y = 0, \quad U_Z = 0, \quad T = T_\infty \tag{5}$$

at $\eta = \infty$, which is at a large distance from the body. Also,

$$\nabla = \boldsymbol{e}_X \frac{\partial}{\partial X} + \boldsymbol{e}_Y \frac{\partial}{\partial Y} + \boldsymbol{e}_Z \frac{\partial}{\partial Z}. \tag{6}$$

The interface is given in general by $\eta(t, X, Y, Z)$, equal to a constant which we shall take to be $\eta = 1$. The energy balance at $\eta = 1$ determines the velocity V_N at which the interface moves; it is given by

$$\rho L V_N = -k \frac{\partial T}{\partial N}, \tag{7}$$

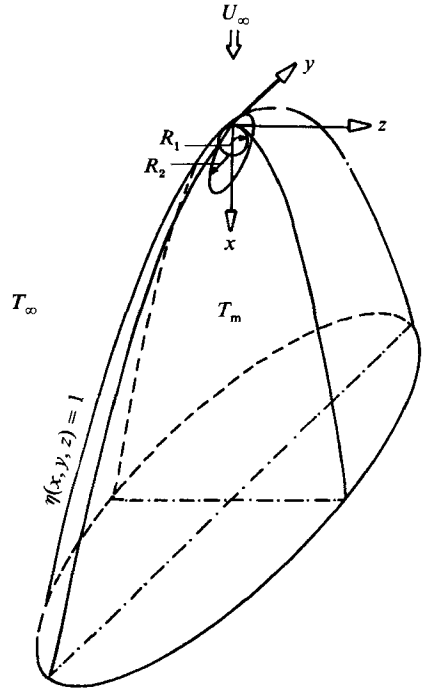

FIGURE 1. Elliptical paraboloid crystal having an aspect ratio, $A = R_2/R_1$. $\eta = 1$ represents the surface of the crystal.

where ν is the kinematic viscosity, α is the thermal diffusivity, ρ is the density of the solid, k is the thermal conductivity of the liquid, N is the direction normal to the interface and where

$$V_N = \left.\frac{-\partial\eta/\partial t}{|\nabla\eta|}\right|_{\eta=1}, \tag{8a}$$

$$|\nabla\eta|^2 = \left(\frac{\partial\eta}{\partial X}\right)^2 + \left(\frac{\partial\eta}{\partial Y}\right)^2 + \left(\frac{\partial\eta}{\partial Z}\right)^2. \tag{8b}$$

Ivantsov (1947) presented an approach to solve (3)–(8), in the absence of convection in the melt, and showed that an isothermal parabolic interface preserves its shape during its growth, because the isotherms in the quiscent melt are also paraboloids. Horvay & Cahn (1961) generalized Ivantsov's solution to the steady growth of an elliptical paraboloid and showed that the elliptical paraboloid crystal also preserves its shape. In this analysis, we shall show that with an Oseen viscous flow in the melt, as depicted in figure 1, an elliptical paraboloidal crystal retains its shape as it grows. First we postulate that the temperature field established by the dissipation of latent heat from the moving interface can be obtained in the form

$$T = T(\eta), \tag{9}$$

where the similarity variable η is

$$\frac{y^2}{A-1+\eta} + \frac{z^2}{\eta} = \eta + 2x \tag{10}$$

and x, y, z are moving coordinates which are related to the fixed coordinates by

$$x = (X + V_G t)/R_1, \quad y = Y/R_1, \quad z = Z/R_1. \tag{11a, b, c}$$

One can derive (10) by using Ivantsov's approach, in which η is found by generalizing (7). This method has been discussed in detail by Ananth (1988), who considered the case of axisymmetric fluid flow over a surface of revolution, and by Ananth & Gill (1984). The aspect ratio is $A = R_2/R_1 > 1$, and R_1 and R_2 are the radii of curvature of the tip, which are the lengthscales that define the size of the dendrite. When η equals a constant, (10) represents the isotherms, and $\eta = 1$ is the surface of an elliptical paraboloidal crystal which grows with a constant velocity, V_G, in the direction of the x-axis. Next, we shall show that (9) and (10) lead to exact solutions of (1)–(8) if one employs the Oseen or Stokes approximations in (2). Furthermore, our analysis demonstrates that the rate of heat transfer from the interface, the rate of growth of the dendrite and the magnitude of the aspect ratio are all interconnected and are profoundly affected by the intensity of the convection in the melt. The connection between convection and the aspect ratio appears to be a subtle but important one.

At steady state, the Oseen form of (1)–(7), relative to an observer moving with the interface, is given as follows:

continuity equation

$$\frac{\partial u}{\partial x}+\frac{\partial v}{\partial y}+\frac{\partial w}{\partial z}=0; \tag{12}$$

momentum equations

$$Re'\frac{\partial u}{\partial x}=-\frac{1}{\rho}\frac{R_1}{\nu}\frac{\partial p}{\partial x}+\left(\frac{\partial^2 u}{\partial x^2}+\frac{\partial^2 u}{\partial y^2}+\frac{\partial^2 u}{\partial z^2}\right), \tag{13}$$

$$Re'\frac{\partial v}{\partial x}=-\frac{1}{\rho}\frac{R_1}{\nu}\frac{\partial p}{\partial y}+\left(\frac{\partial^2 v}{\partial x^2}+\frac{\partial^2 v}{\partial y^2}+\frac{\partial^2 v}{\partial z^2}\right), \tag{14}$$

$$Re'\frac{\partial w}{\partial x}=-\frac{1}{\rho}\frac{R_1}{\nu}\frac{\partial p}{\partial z}+\left(\frac{\partial^2 w}{\partial x^2}+\frac{\partial^2 w}{\partial y^2}+\frac{\partial^2 w}{\partial z^2}\right); \tag{15}$$

energy equation

$$u\frac{\partial T}{\partial x}+v\frac{\partial T}{\partial y}+w\frac{\partial T}{\partial z}=\frac{\alpha}{R_1}\left(\frac{\partial^2 T}{\partial x^2}+\frac{\partial^2 T}{\partial y^2}+\frac{\partial^2 T}{\partial z^2}\right). \tag{16a}$$

Substituting (9) and (10) into (16a), we obtain

$$\frac{\mathrm{d}^2 T}{\mathrm{d}\eta^2}+f(\eta)\frac{\mathrm{d}T}{\mathrm{d}\eta}=0, \tag{16b}$$

where

$$f(\eta)=\frac{1}{2\eta}+\frac{1}{2(A-1+\eta)}-\frac{R_1}{2\alpha\eta}\left\{-u\eta+\frac{vy\eta}{A-1+\eta}+wz\right\}. \tag{16c}$$

The precise dependence of f on η and the system parameters will be given later, in (26).

In addition to (16) the boundary conditions are

$$u=V_G,\quad v=0,\quad w=0,\quad T=T_m\quad \text{at } \eta=1, \tag{17}$$

$$u=U_\infty+V_G,\quad v=0,\quad w=0,\quad T=T_\infty\quad \text{at } \eta=\infty, \tag{18}$$

and Re' is defined by

$$Re'=Re+\frac{V_G R_1}{\nu}, \tag{19}$$

where the Reynolds number is $Re = U_\infty R_1/\nu$, and p is the pressure. u, v, w are the fluid velocity components in the x-, y-, z-directions measured relative to an observer

moving with the interface. They are related to the fluid velocities measured with respect to the fixed coordinates by

$$u = V_G + U_x, \quad v = U_Y, \quad w = U_Z, \quad p = P, \tag{20a, b, c, d}$$

where V_G is the steady-state growth velocity of the interface.

As shown in Appendix A the fluid velocities, u, v, w, measured relative to a moving observer, are given by

$$u = U_\infty + V_G - \frac{2U_\infty}{\left\{\left(\frac{y}{A-1+\eta}\right)^2 + \left(\frac{z}{\eta}\right)^2 + 1\right\}}\left\{\frac{\exp\left(-\frac{1}{2}Re'\right) - \exp\left(-\frac{1}{2}Re'\eta\right)}{CRe'[\eta(A-1+\eta)]^{\frac{1}{2}}}\right\}$$
$$- \frac{U_\infty}{C}\int_\eta^\infty \frac{\exp\left(-\frac{1}{2}Re'\eta\right)}{[\eta(A-1+\eta)]^{\frac{1}{2}}}\,d\eta, \tag{21}$$

$$v = \frac{2yU_\infty}{(A-1+\eta)\left\{\left(\frac{y}{A-1+\eta}\right)^2 + \left(\frac{z}{\eta}\right)^2 + 1\right\}}\left\{\frac{\exp\left(-\frac{1}{2}Re'\right) - \exp\left(-\frac{1}{2}Re'\eta\right)}{CRe'[\eta(A-1+\eta)]^{\frac{1}{2}}}\right\}, \tag{22}$$

$$w = \frac{2zU_\infty}{\left\{\left(\frac{y}{A-1+\eta}\right)^2 + \left(\frac{z}{\eta}\right)^2 + 1\right\}\eta}\left\{\frac{\exp\left(-\frac{1}{2}Re'\right) - \exp\left(-\frac{1}{2}Re'\eta\right)}{CRe'[\eta(A-1+\eta)]^{\frac{1}{2}}}\right\}, \tag{23}$$

and the pressure is given by

$$p = \frac{2}{C}\left(\frac{\rho\nu}{R_1}\right)\frac{U_\infty}{\left\{\left(\frac{y}{A-1+\eta}\right)^2 + \left(\frac{z}{\eta}\right)^2 + 1\right\}}\frac{\exp\left(-\frac{1}{2}Re'\right)}{[\eta(A-1+\eta)]^{\frac{1}{2}}}, \tag{24a}$$

where

$$C = \int_1^\infty \frac{\exp\left(-\frac{1}{2}Re'\eta\right)}{[\eta(A-1+\eta)]^{\frac{1}{2}}}\,d\eta. \tag{24b}$$

The velocity components u, v, w, and pressure p, which are given explicitly by (21)–(24a) were derived here in a relatively simple way by using Ivantsov's approach. In contrast, the procedure described by Wilkinson (1955) involves laborious coordinate transformations and assumes that the interface is stationary.

The thermal field is obtained by integrating (16b) with the boundary conditions for temperature given by (17) and (18). The result is

$$\theta = \frac{T - T_\infty}{T_m - T_\infty} = \frac{\int_\eta^\infty \exp\left[-\int_1^\eta f\,d\eta\right]d\eta}{\int_1^\infty \exp\left[-\int_1^\eta f\,d\eta\right]d\eta}, \tag{25}$$

where f is a function of η and the parameters are the Reynolds number Re, the growth Péclet number P_G, the Prandtl number Pr, and the aspect ratio A. The function f, which is determined by substituting (21)–(24) into (16c), is given explicitly by

$$f(\eta; Pe, A, P_G, Pr) = \tfrac{1}{2}(P_G + Pe) + \frac{1}{2}\left\{\frac{1}{\eta} + \frac{1}{A(1+(\eta-1)/A)}\right\}$$
$$\frac{Pe}{Re'[\eta(1+(\eta-1)/A)]^{\frac{1}{2}}}\left\{\frac{\exp\left(-\frac{1}{2}Re'\right) - \exp\left(-\frac{1}{2}Re'\eta\right)}{\int_1^\infty \frac{\exp\left(-\frac{1}{2}Re'\eta\right)}{[\eta(1+(\eta-1)/A)]^{\frac{1}{2}}}\,d\eta}\right\} - \tfrac{1}{2}Pe\frac{\int_\eta^\infty \frac{\exp\left(-\frac{1}{2}Re'\eta\right)}{[\eta(1+(\eta-1)/A)]^{\frac{1}{2}}}\,d\eta}{\int_1^\infty \frac{\exp\left(-\frac{1}{2}Re'\eta\right)}{[\eta(1+(\eta-1)/A)]^{\frac{1}{2}}}\,d\eta} \tag{26}$$

Equation (26) is of central importance in this analysis because it determines: (i) the behaviour of the thermal field in the neighbourhood of the dendrite, (ii) the heat transfer characteristics of the system, and (iii) the fact that Oseen viscous flow and translating elliptical paraboloidal interfaces which generate latent heat are compatible with one another.

The heat flux balance at the interface, given by (7), can be written as

$$\rho L V_{\mathrm{N}} = -k(\nabla T \cdot \boldsymbol{N}), \tag{27}$$

where $\boldsymbol{N}$ is the vector normal to the interface and is given by

$$\boldsymbol{N} = \frac{\nabla \eta}{|\nabla \eta|}. \tag{28}$$

By substituting (8a), (9) and (28) into (27) we get

$$\frac{\partial \eta / \partial t}{|\nabla \eta|^2_{\eta=1}} = \frac{k}{\rho L} \frac{\mathrm{d}T(1)}{\mathrm{d}\eta}, \tag{29}$$

where η and its partial derivatives in (27)–(29) are evaluated with respect to the fixed coordinates X, Y, Z. Equations (10) and (11) when substituted into (29) yield

$$Nu = \frac{P_{\mathrm{G}}}{St} = -2 \frac{\mathrm{d}\theta}{\mathrm{d}\eta}(1) \tag{30}$$

and substituting (25) into (30) gives

$$Nu = \frac{P_{\mathrm{G}}}{St} = \frac{2}{\displaystyle\int_1^{\infty} \exp\left[-\int_1^{\eta} f(\eta; Re, A, P_{\mathrm{G}}, Pr)\, \mathrm{d}\eta \right] \mathrm{d}\eta}, \tag{31a}$$

$$Nu = Nu(Re, A, P_{\mathrm{G}}, Pr), \tag{31b}$$

$$Nu_{\mathrm{s}} = Nu/[1 + (y/A)^2 + z^2]^{\frac{1}{2}}, \tag{31c}$$

where the Nusselt number at the tip is $Nu = hR_1/k$, h is the heat transfer coefficient, and Nu_{s} is the Nusselt number anywhere on the solid surface. Also, $St = (T_{\mathrm{m}} - T_{\infty})/(L/C_p)$, $Re = U_{\infty} R_1/\nu$, $P_{\mathrm{G}} = V_{\mathrm{G}} R_1/\alpha$ and $Pr = \nu/\alpha$. Equation (31a) is the principal result of this analysis. The paraboloid of revolution ($A = 1$), which was studied by Ananth & Gill (1988a), and the parabolic cylinder ($A = \infty$) occur as special cases of (31a). In the next section we shall show that the shape (aspect ratio) has a particularly large effect on heat transfer at low Reynolds numbers.

The results of Ananth & Gill (1988b) for axisymmetric thermal convection with $A = 1$ are similar to (31b) except that Re is replaced by Gr. In the axisymmetric thermal convection case, without making additional assumptions, one can make direct comparisons between the mathematical results and the experimental data on succinonitrile for the growth velocity and tip radius as functions of ΔT in the form $V_{\mathrm{G}} = V_{\mathrm{G}}(\Delta T)$ and $R = R(\Delta T)$.

3. Results and discussion

Equation (31) is the convective analogue of the pure conduction solution of Horvay & Cahn for the growth of an isothermal elliptical paraboloid which preserves its shape as it grows. Our solution shows that an elliptical paraboloid also preserves its shape in the presence of Oseen viscous flow. This is in agreement with the

observations of Chang & Gill (1987) whose double-exposure photographs show that the shape of a dendrite of ice is preserved in the presence of forced flow up to five side branches from the tip, which appears to be approximated best by an elliptical paraboloid. Therefore, it seems that the effects of anisotropic attachment kinetics and surface tension, which we have not taken into account in the preceding analysis create only small deviations in the actual shape of the tip region of dendrites from that of an elliptical paraboloid, and yet these anisotropic effects may be crucial in selecting particular values of R_1 and R_2 and V_G, for fixed values of ΔT and U_∞.

The primary driving force for growth is the subcooling. If St is zero, no growth takes place. However, for finite values of St the intensity of convection, as indicated by the value of Re, can influence the growth rate profoundly. Furthermore the interactions among the parameters can be very complex. Therefore, our goal now is to illustrate how the various transport mechanisms (convection, conduction, apparent convection due to the moving boundary) compete for dominance in the growth process. We also hope to demonstrate how shape, as reflected in A, favours one mechanism or the other.

At this point it seems desirable to try to make clear what we mean by the distinction between 'real' and 'apparent' convection. Real convection is measured by Re and it occurs only when the melt is in motion. Apparent convection is measured by P_G, which reflects the motion of the interface and augments heat transfer, as does Re, but the effect is autocatalytic in the sense that the solutions given by (31a) define the set $P_G = P_G(A, Re, St, Pr)$.

Figure 2 displays the solutions given by (31a) for the ice–water system ($Pr = 13.5$) in the form P_G versus St, with A and Re as parameters. Clearly, A and Re have a significant effect on P_G, and this effect is more pronounced when the subcooling, as reflected by St, is small and the effect of the moving boundary, compared to that of convection in the melt, is small. As the intensity of convection increases, the effect of the moving boundary becomes less significant ($Pe \gg P_G$), and the right-hand side of (31a) becomes independent of P_G. Therefore, P_G varies linearly with St, as shown by the fact that lines (a)–(d) in figure 2 are straight at small St and large Re, and P_G/St is independent of St.

Figure 3 shows that the effect of A on P_G decreases as Re increases. For example at $Re = 1$ an increase in A beyond 10 does not affect P_G significantly as shown by curve (e) of figure 3.

Figure 4 shows two photographs of ice crystals grown in a quiescent melt which is at a $\Delta T = 0.3$ K. In figure 4(a) a double-exposure photograph indicates that the shape is preserved between exposures and one sees that the tip of the dendrite is split because it had become unstable at an earlier time. Figure 4(b) displays the same dendrite at a later time at which it has reorganized itself and a new stable tip has been generated. The deep vertical indentation on the left-hand side of the main stem is a result of the tip splitting event which had occurred earlier and is shown in figure 4(a). The tip radius R_2 of the fully developed dendrite in figure 4(b) is about 200 μm which is 100 times the value of R_1 given by Kallungal.

Our self-consistent analysis of the flow and energy equations yields a solution which includes a shape that is very close to the one observed in ice experiments illustrated in figure 4(b) and those that will be discussed subsequently. Therefore, one would expect that the thermal field and the heat transfer rates in the liquid phase given by (25) and (31a) are reasonable approximations, especially at the tip where attachment kinetics are very rapid along the A-axis and the melting point depression due to capillarity is less than 4% as indicated by Kind *et al.* (1987) for the ice–water

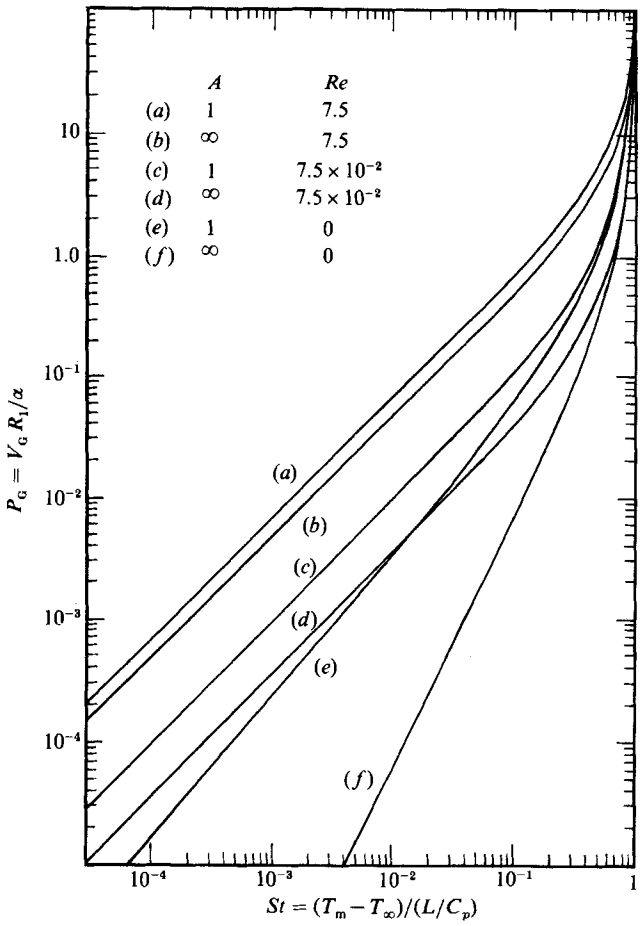

FIGURE 2. Effect of Reynolds number $Re = U_\infty R_1/\nu$, and the aspect ratio $A = R_2/R_1$, on growth Péclet number P_G, as a function of Stefan number St. $Pr = \nu/\alpha = 13.5$.

system. On the other hand, as assumed by Fujioka & Sekerka (1974), slow interfacial kinetics may inhibit growth along the c-axis, especially downstream from the tip, and this decreases the interfacial temperature, which would induce heat conduction in the solid phase back from the tip, and may result in higher growth Péclet numbers than are given by (31 a), which is derived assuming that the solid phase is isothermal. The lack of experimental data for the kinetic coefficient, which is anisotropic, makes it difficult to estimate the appropriate lengthscale for the solid-phase conduction and hence its contribution to the growth rate of the tip. As a result, we have chosen to examine (31 a) by using the experimental data of Kallungal & Barduhn, and Chang & Gill and this may give some hint regarding the importance of kinetic resistance. Several alternatives are available for making these comparisons between our theory and the experimental data. However, considering the uncertainty in the R_1 and R_2 data, none of these approaches is expected to yield definitive results. We have tried to choose an approach that is sensitive to small changes in the measured quantities and one which therefore will emphasize differences between the experiments and theory. Thus we plot P_G/St as a function of Re by using (31 a) for various values of A and St. If one also plots Kallungal's data on the same graph then the combination of

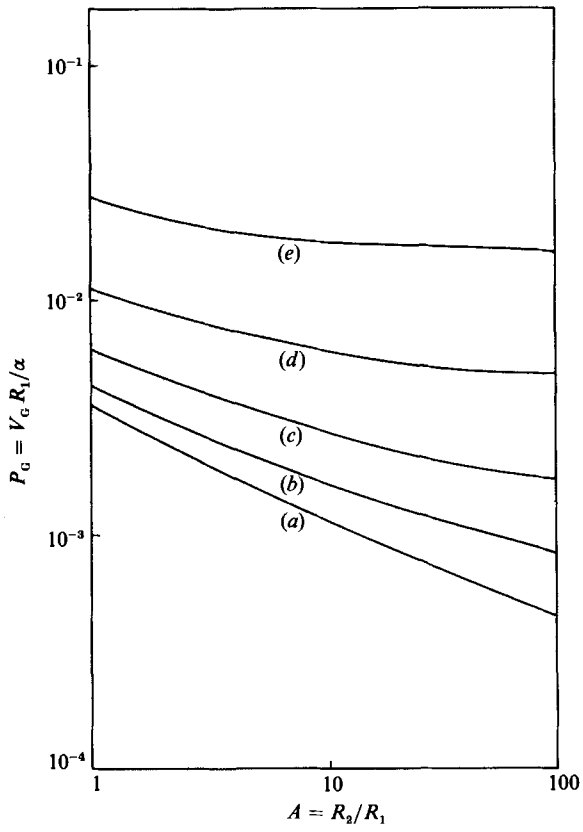

FIGURE 3. The effect of shape on the growth Péclet number at various levels of convection in the melt, *Re*: (*a*) $Re = 0$; (*b*) 1×10^{-3}; (*c*) 1×10^{-2}; (*d*) 1×10^{-1}; (*e*) 1.0. $St = 1 \times 10^{-2}$, $\Delta T = 0.8$ °C, $Pr = 13.5$.

theoretical and experimental results yields a value of A, which gives a value of R_2 that can be compared with the experimental data reported by Chang. These comparisons and their implications are discussed in this section with the intention of gaining some insight into the effect of convection in the melt on the interaction among the various parameters and their affect on the growth process.

Kallungal (1974) measured the aspect ratio and reported it to be about 100 at small values of *Re*, which is consistent with our figure 4. The data points of Kallungal, for three different subcoolings are shown on figure 5, and they agree quite well with the theory when *Re* is less than about 10^{-3}. This suggests that the shape of the ice dendrite tip is not changed significantly by the introduction of a small amount of convection. This seems to agree with the fact that the succinonitrile dendritic tip ($A = 1$) remains approximately parabolic despite the presence of thermal convection of the order of $Gr \approx 10^{-4}$ (Ananth & Gill 1988*b*) in the experiments of Huang & Glicksman (1981) and Glicksman & Huang (1982). As *Re* increases above 10^{-3}, however, the theoretical results for $A = 100$ shown in figure 5 underpredict the ice data, which may be due to a decrease in A as *Re* increases. This effect of *Re* on A is in accord qualitatively with the experimental data of Chang (1985) which shows that R_2 decreases as *Re* increases. Figure 5 also shows that the effect of convection on P_G becomes significant when *Re* gets larger than 10^{-5}.

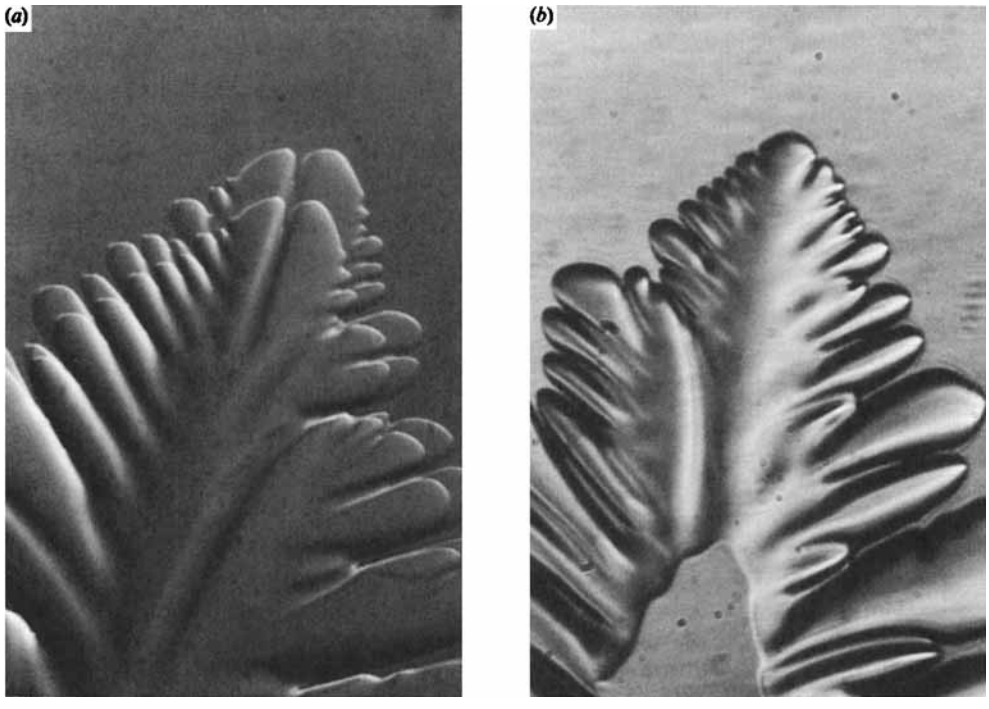

FIGURE 4. The double-exposure photographs, shown on (*a*), indicate the shape-preserving nature of dendritic growth. (*b*) Shows a photograph of the same steadily growing stable tip taken at a later time.

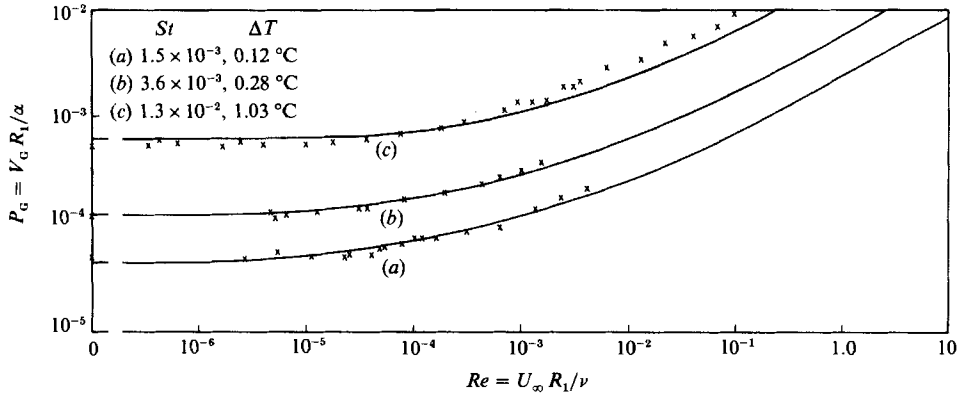

FIGURE 5. Comparison of the theory (——) for growth Péclet number as a function of Reynolds number with the ice data of Kallungal (×) at aspect ratio = 100. $Pr = 13.5$.

Figure 6 illustrates the competition between the augmentation of the heat transfer rate by the moving boundary and by convection in the melt. When the subcooling is on the order of 1 °C or less, the effect of the moving boundary on Nu becomes small as Re gets larger than 10^{-4}, and it is negligible for Re larger than 10^{-3}. Therefore, the Nusselt number becomes a function only of A and Re, so that $Nu = Nu(A, Re)$ for $Re > 10^{-3}$. This implies that theories based on a stationary configuration, such as that of Dash & Gill (1984), give reasonable results when convection in the melt dominates the moving-boundary effect.

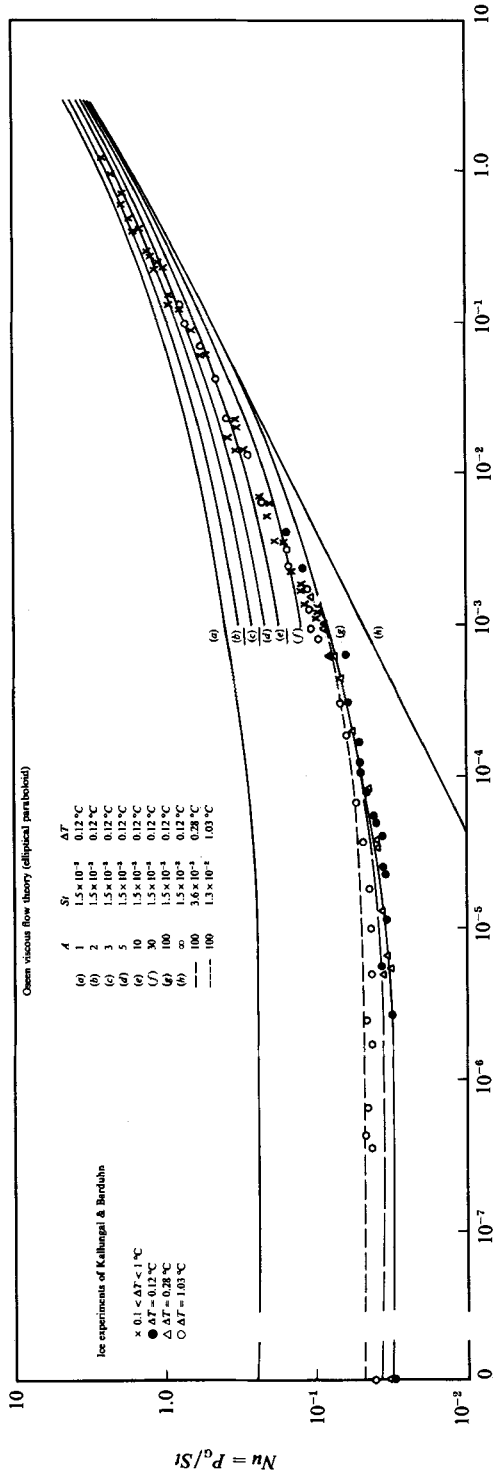

FIGURE 6. Comparison of the predicted values of the Nusselt number for various values of aspect ratio as a function of Reynolds number with the ice data.

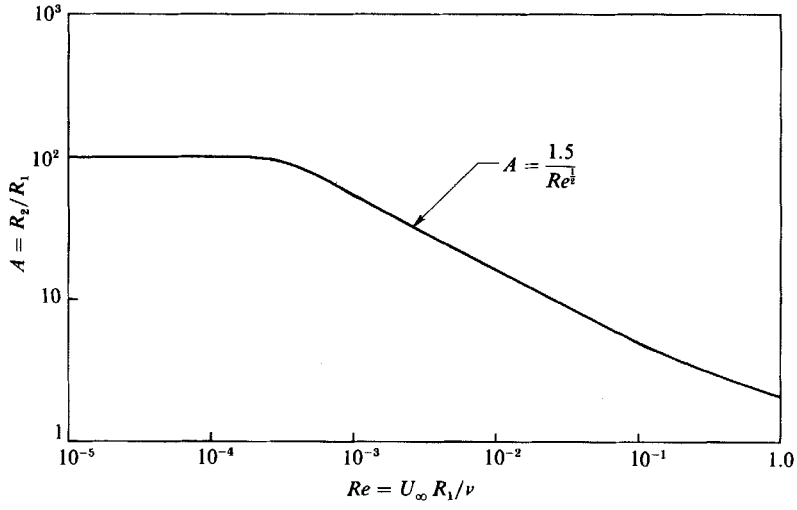

FIGURE 7. Variation of aspect ratio with Reynolds number. Obtained from the comparisons between theory and Kallungal–Barduhn data on ice shown in figure 6. $Pr = 13.5$.

The predicted values of Nu as a function of Re are shown on figure 6 for various values of A. The experimental data points (Nu, Re) of Kallungal, when plotted on figure 6, correspond to various values of the aspect ratio A as a function of Re. The resulting values of A, which are displayed on figure 7, show that the tip of an ice dendrite becomes more symmetric (A decreases) and tends towards a paraboloid of revolution as Re is increased. The reasons why the aspect ratio decreases with increasing Re have not been established, but they probably are related to the anisotropic Gibbs–Thompson capillarity and surface kinetics, which we have not included in the present analysis.

Since $A = R_2/R_1$ we can calculate R_2 by using Kallungal's values of R_1, which he found to be insensitive to Re, at least up to $Re \sim 0.1$. Therefore, figure 7 suggests that R_2 decreases as Re increases and this behaviour is in qualitative agreement with the experimental data of Chang as shown in figure 8. Figure 8 also shows that the values of R_2 indicated by the theory are too small at large values of Re and too large at small values of Re. This quantitative discrepancy between the combination of our theory with the data of Kallungal and the values of R_2 which Chang observed may stem from two sources:

(i) Small errors in the measurements of R_1 and V_G create errors in P_G which lead to larger errors in the calculated values of A because, as shown in figures 3 and 6, P_G becomes less sensitive to changes in A as the Reynolds number increases and approaches 1.

(ii) Interfacial kinetic resistance to growth in the direction of the c-axis, which has been discussed by Fujioka & Sekerka (1974), and the capillarity effect at the tip, may be responsible for the difference between the calculated and observed values of R_2. Kinetic resistance becomes more important as Re increases and heat transfer rates become inherently larger. This causes the temperature of the surface of the basal plane to approach T_∞ because of kinetic undercooling. Therefore conduction is induced in the solid phase from the tip to the rear of the dendrite and this increases the growth rate. The omission of this effect in the theory would manifest itself in a predicted value of P_G which is too small if the correct experimental value of A were used. Therefore when we combine Kallungal's experiments with our theory we may

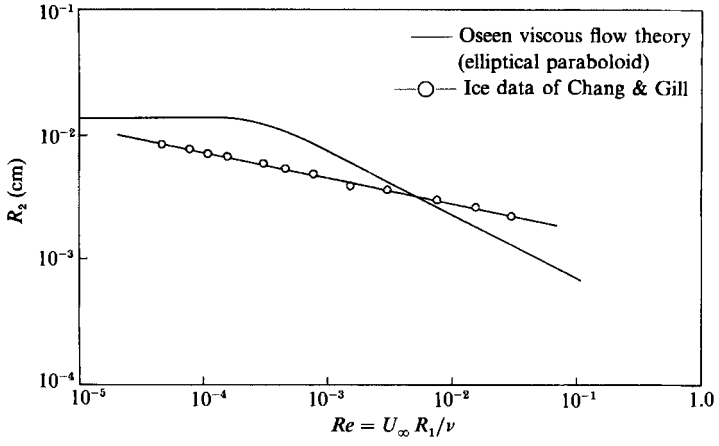

FIGURE 8. Comparison of estimated values of tip radius measured parallel to the basal plane, R_2, as a function of Reynolds number with the data on ice of Chang & Gill. $\Delta T = 0.44$ °C, $Pr = 13.5$.

get a calculated value of A which is too small in order to enable the theory to compensate for the omission of the kinetic resistance. On the other hand when Re is small, and heat transfer rates are inherently smaller, kinetics may not be as important and kinetic undercooling would be smaller. If this is the case, capillarity can induce solid-phase heat conduction toward the tip and reduce heat transfer to the melt. This Gibbs–Thompson effect inhibits the growth rate and may account for the theory indicating values of A that are too large at small values of Re.

4. Conclusions

Our analysis leads to the following conclusions:

(i) Self-consistent solutions to the Navier–Stokes and energy equations can be obtained for isothermal elliptical paraboloids if the Oseen viscous flow approximation is made.

(ii) As Re increases and convection intensifies, the effect of aspect ratio on the growth Péclet number P_G becomes less significant.

(iii) The effect of the moving boundary on the growth rate of the dendrite tip becomes negligible for $Pe \gg P_G$, in which case P_G varies linearly with St. This occurs when $\Delta T < 1$ °C and $Re > 10^{-3}$ in the case of ice dendrites.

(iv) Comparison of the theoretical solutions with the experimental data of Kallungal (1974) indicates that A, for the growth of ice in water subcooled to $\Delta T \lesssim 1$ °C, decreases, as illustrated in figure 7, as Re increases beyond 10^{-3}. This is in agreement qualitatively with the experimental data of Chang (1985). More precise experiments and a full theory which accounts for the anisotropic effects are needed for quantitative understanding of ice crystal growth at large Re.

This work was supported in part by NSF Grants CBT8506585, 8513606 and 8796343.

Note added in proof. After this article was submitted for publication, an article appeared by Saville & Beaghton (1988) which extends the solution of Dash & Gill (1984) for Oseen forced viscous flow over a paraboloid of revolution to the case of a moving interface considered by Gill *et al.* (1987) and Ananth & Gill (1988*a*). The

methods used are different, and Saville & Beaghton appear to have used directly the Oseen velocity profiles of Wilkinson (1955) which are for stationary paraboloids. Therefore, their equation (2.20) seems to be approximate and different from the exact solution given in equation (49) of Ananth & Gill (1988*a*). Also, no comparisons with experimental data were made by Saville & Beaghton.

Appendix A

The fluid velocity components, u, v, w, measured with respect to an observer moving with the solid–liquid interface, are obtained by solving (12)–(15) with the boundary conditions (17) and (18) given in the text. Let

$$u = U_\infty + V_G - u', \tag{A 1}$$

$$v = -v', \tag{A 2}$$

$$w = -w', \tag{A 3}$$

where u', v', w' are the perturbed velocity components along the directions x-, y-, z-, respectively. By substituting (A 1)–(A 3) into (12)–(15), (17) and (18), we get

$$\frac{\partial u'}{\partial x} + \frac{\partial v'}{\partial y} + \frac{\partial w'}{\partial z} = 0, \tag{A 4}$$

$$Re' \frac{\partial u'}{\partial x} = \frac{1}{\rho} \frac{R_1}{\nu} \frac{\partial p}{\partial x} + \left(\frac{\partial^2 u'}{\partial x^2} + \frac{\partial^2 u'}{\partial y^2} + \frac{\partial^2 u'}{\partial z^2} \right), \tag{A 5}$$

$$Re' \frac{\partial v'}{\partial x} = \frac{1}{\rho} \frac{R_1}{\nu} \frac{\partial p}{\partial y} + \left(\frac{\partial^2 v'}{\partial x^2} + \frac{\partial^2 v'}{\partial y^2} + \frac{\partial^2 v'}{\partial z^2} \right), \tag{A 6}$$

$$Re' \frac{\partial w'}{\partial x} = \frac{1}{\rho} \frac{R_1}{\nu} \frac{\partial p}{\partial z} + \left(\frac{\partial^2 w'}{\partial x^2} + \frac{\partial^2 w'}{\partial y^2} + \frac{\partial^2 w'}{\partial z^2} \right). \tag{A 7}$$

The boundary conditions become

$$u' = U_\infty, \quad v' = w' = 0 \quad \text{at} \quad \eta = 1, \tag{A 8}$$

$$u' = v' = w' = 0 \quad \text{at} \quad \eta = \infty. \tag{A 9}$$

If functions $M(\eta)$ and $N(\eta)$ are defined such that

$$u' = \left(\frac{\mathrm{d}M}{\mathrm{d}\eta} + \frac{1}{Re'} \frac{\mathrm{d}N}{\mathrm{d}\eta} \right) \frac{\partial \eta}{\partial x} - N(\eta), \tag{A 10}$$

$$v' = \left(\frac{\mathrm{d}M}{\mathrm{d}\eta} + \frac{1}{Re'} \frac{\mathrm{d}N}{\mathrm{d}\eta} \right) \frac{\partial \eta}{\partial y}, \tag{A 11}$$

$$w' = \left(\frac{\mathrm{d}M}{\mathrm{d}\eta} + \frac{1}{Re'} \frac{\mathrm{d}N}{\mathrm{d}\eta} \right) \frac{\partial \eta}{\partial z}, \tag{A 12}$$

and

$$p = \frac{\rho \nu}{R_1} Re' \frac{\mathrm{d}M}{\mathrm{d}\eta} \frac{\partial \eta}{\partial x}, \tag{A 13}$$

then (A 4)–(A 9) can be reduced to the following form by substituting (A 10)–(A 13) into them:

$$\frac{\mathrm{d}^2M}{\mathrm{d}\eta^2}+\frac{\nabla^2\eta}{|\nabla\eta|^2}\frac{\mathrm{d}M}{\mathrm{d}\eta}=0, \tag{A 14}$$

$$\frac{\mathrm{d}^2N}{\mathrm{d}\eta^2}+\frac{(\nabla^2\eta-Re'\,\partial\eta/\partial x)}{|\nabla\eta|^2}\frac{\mathrm{d}N}{\mathrm{d}\eta}=0, \tag{A 15}$$

where

$$\nabla^2\eta=\frac{\partial^2\eta}{\partial x^2}+\frac{\partial^2\eta}{\partial y^2}+\frac{\partial^2\eta}{\partial z^2}, \quad |\nabla\eta|^2=\left(\frac{\partial\eta}{\partial x}\right)^2+\left(\frac{\partial\eta}{\partial y}\right)^2+\left(\frac{\partial\eta}{\partial z}\right)^2,$$

η is given by (10), and M, N are functions of η only.

By substituting (10) into (A 14) and (A 15) we obtain

$$\frac{\mathrm{d}^2M}{\mathrm{d}\eta^2}+\frac{1}{2}\left\{\frac{1}{\eta}+\frac{1}{(A-1+\eta)}\right\}\frac{\mathrm{d}M}{\mathrm{d}\eta}=0, \tag{A 16}$$

$$\frac{\mathrm{d}^2N}{\mathrm{d}\eta^2}+\frac{1}{2}\left\{Re'+\frac{1}{\eta}+\frac{1}{(A-1+\eta)}\right\}\frac{\mathrm{d}N}{\mathrm{d}\eta}=0. \tag{A 17}$$

Integration of (A 16) and (A 17) yields

$$M=C_1\int_1^{\eta}\frac{1}{[\eta(A-1+\eta)]^{\frac{1}{2}}}\mathrm{d}\eta+C_2 \tag{A 18}$$

and

$$N=-C_3\int_{\eta}^{\infty}\frac{\exp\left(-\frac{1}{2}Re'\,\eta\right)}{[\eta(A-1+\eta)]^{\frac{1}{2}}}\mathrm{d}\eta+C_4, \tag{A 19}$$

where C_1, C_2, C_3, C_4 are the constants of integration. These constants can be evaluated by substituting (A 18) and (A 19) into (A 10)–(A 13) for the perturbed velocities and using the boundary conditions (A 8) at $\eta = 1$ and (A 9) at $\eta = \infty$. The resulting solutions are given by (21)–(24).

Appendix B. Stokes flow solution for the growth of an elliptical paraboloid

The flow field is given by

$$u=V_{\mathrm{G}}-\frac{qA^{\frac{1}{2}}}{\left\{\left(\frac{y}{A-1+\eta}\right)^2+\left(\frac{z}{\eta}\right)^2+1\right\}}\left\{\frac{\eta-1}{[\eta(A-1+\eta)]^{\frac{1}{2}}}\right\}+q\int_1^{\eta}\frac{\mathrm{d}\eta}{\left[\eta\left(1+\frac{\eta-1}{A}\right)\right]^{\frac{1}{2}}} \tag{B 1}$$

$$v=\frac{yqA^{\frac{1}{2}}}{(A-1+\eta)\left\{\left(\frac{y}{(A-1+\eta)}\right)^2+\left(\frac{z}{\eta}\right)^2+1\right\}}\left\{\frac{\eta-1}{[\eta(A-1+\eta)]^{\frac{1}{2}}}\right\} \tag{B 2}$$

$$w=\frac{zqA^{\frac{1}{2}}}{\left\{\left(\frac{y}{A-1+\eta}\right)^2+\left(\frac{z}{\eta}\right)^2+1\right\}\eta}\left\{\frac{\eta-1}{[\eta(A-1+\eta)]^{\frac{1}{2}}}\right\}. \tag{B 3}$$

The pressure is given by

$$p = 2\left(\frac{\rho\nu}{R_1}\right)\frac{q}{\left\{\left(\frac{y}{A-1+\eta}\right)^2+1+\left(\frac{z}{\eta}\right)^2\right\}}\frac{A^{\frac{1}{2}}}{[\eta(A-1+\eta)]^{\frac{1}{2}}}, \tag{B 4}$$

and

$$f(\eta) = \frac{1}{2}\left\{P_G+\frac{1}{\eta}+\frac{1}{(A-1+\eta)}\right\}-\frac{R_1 q}{2\alpha}\frac{(\eta-1)A^{\frac{1}{2}}}{[\eta(A-1+\eta)]^{\frac{1}{2}}}+\frac{R_1 q}{2\alpha}\int_1^\eta \frac{\mathrm{d}\eta}{\left[\eta\left(1+\frac{\eta-1}{A}\right)\right]^{\frac{1}{2}}} \tag{B 5}$$

where

$$\int_1^\eta \frac{\mathrm{d}\eta}{\left[\eta\left(1+\frac{\eta-1}{A}\right)\right]^{\frac{1}{2}}} = 2A^{\frac{1}{2}}\ln\left(\frac{\eta^{\frac{1}{2}}+[A-1+\eta]^{\frac{1}{2}}}{1+A^{\frac{1}{2}}}\right).$$

The thermal field and Nusselt number are given by (25) and (31*a*) respectively. Equations (B 1)–(B 5) satisfy the differential equations (12) to (16) with Re appearing on the left hand sides of equations (13)–(15) being replaced by $V_G R_1/\alpha$. They also satisfy the boundary condition at the surface ($\eta = 1$) given by (17) but not the far-field condition. Therefore, the Stokes solution is valid only up to a distance $\eta \approx 2/Re'$ from the surface. By matching equations (B 1)–(B 5) with the Oseen solution given by (21)–(24), and (26) to the order Re' for small Re and for $\eta < 2/Re'$ the constant 'q' is determined as

$$q = \frac{U_\infty}{\int_1^\infty \frac{\exp(-Re'\eta/2)}{\left[\eta\left(1+\frac{\eta-1}{A}\right)\right]^{\frac{1}{2}}}}. \tag{B 6}$$

As noted in the Introduction, the Oseen approximation to the Navier–Stokes equations become inaccurate as $A \to \infty$ and the body becomes a parabolic cylinder. Therefore, equation (B 6) becomes inaccurate and yields $q = 0.8U_\infty(Re')^{\frac{1}{2}}$, for parabolic cylinders, instead of $q = 0.53U_\infty(Re')^{\frac{1}{2}}$ which is obtained by using the numerical solutions of the Navier–Stokes equations given by Davis (1972).

Clearly the Oseen solution, equations (21)–(24) and (26), reduces to Stokes' solution, (B 1)–(B 6), close to the solid surface when Re' is small ($Re \to 0$ and $\eta \ll 2/Re'$). Therefore, both the Oseen and Stokes approximations yield the same results for the thermal field and the Nusselt number, for small Re' and large Pr, because the thermal boundary layers are thin.

REFERENCES

Ananth, R. 1988 Dendritic crystal growth with convection in the melt, Chap. 3. Ph.D. dissertation, SUNY at Buffalo, Buffalo, NY.

Ananth, R. & Gill, W. N. 1984 *J. Cryst. Growth* **70**, 24.

Ananth, R. & Gill, W. N. 1988*a* *Chem. Engng Commun.* **68**, 1.

Ananth, R. & Gill, W. N. 1988*b* *J. Cryst. Growth* **91**, 587.

Cantor, B. & Vogel, A. 1977 *J. Cryst. Growth* **41**, 109.

Chang, L.-Y. 1985 Dynamics and steady-state process of crystal growth in quiescent and flowing systems. Ph.D. dissertation, SUNY at Buffalo, Buffalo, NY.

Chang, L. & Gill, W. N. 1987 *AIChE Annual Meeting, New York, NY, Nov. Paper* 103g.

Dash, S. K. & Gill, W. N. 1984 *Intl J. Heat Mass Transfer* **27**, 1345.

DAVIS, R. T. 1972 *J. Fluid Mech.* **51**, 417.

DAVIS, R. T. & WERLE, M. J. 1972 *AIAA J.* **10**, 1224.

DENNIS, S. R. C. & WALSH, J. D. 1971 *J. Fluid Mech.* **50**, 801.

DOHERTY, R. D., CANTOR, B. & FAIRS, S. 1978 *Metall. Trans.* **9A**, 621.

FERNANDEZ, R. & BARDUHN, A. J. 1967 *Desalination* **3**, 330.

FUJIOKA, T. 1978 Study of ice growth on slightly undercooled water. Ph.D. dissertation, Carnegie-Mellon University, Pittsburgh, PA.

FUJIOKA, T. & SAKERKA, R. F. 1974 *J. Cryst. Growth* **24/25**, 84.

GILL, W. N., ANANTH, R. & TIRMIZI, S. H. 1987 *Joint Summer Research Conf. on Crystal Growth and Pattern Formation in Phase Transition, July 26 to August 1, Cornell University, Ithaca, NY.* American Mathematical Society.

GLICKSMAN, M. E. & HUANG, S. C. 1982 In *Convective Transport and Instability Phenomena* (ed. J. Zierep and H. Oertel), p. 3.2.2. Karlsruhe: Braun.

HORVAY, G. & CAHN, J. W. 1961 *Acta Metall.* **9**, 695.

HUANG, J. S. 1975 The effect of natural convection in ice crystal growth in salt solutions. Ph.D. dissertation, Syracuse University, Syracuse, NY.

HUANG, J. S. & BARDUHN, A. J. 1985 *AIChE J.* **36**, 749.

HUANG, S. C. & GLICKSMAN, M. E. 1981 *Acta Metall.* **29**, 701; 717.

IVANTSOV, G. P. 1947 *Dokl. Akad. Nauk USSR* **58**, 567. (Translation by Horvay, G. 1960 *General Electric Rep.* 60-RL-2511M.)

KALLUNGAL, J. P. 1974 The growth of a single ice crystal parallel to the A-axis in subcooled quiescent and flowing water. Ph.D. dissertation, Syracuse University, Syracuse, NY.

KALLUNGAL, J. P. & BARDUHN, A. J. 1977 *AIChE J.* **23**, 294.

KIND, M., GILL, W. N. & ANANTH, R. 1987 *Chem. Engng Commun.* **55**, 295.

LAGERSTROM, P. A. 1964 *High Speed Aerodynamics and Jet Propulsion*, vol. IV (ed. F. K. Moore), chap. 2. Princeton University Press.

LAGERSTROM, P. A. & COLE, J. D. 1955 *J. Rat. Mech. Anal.* **4**, 817.

SAVILLE, D. A. & BEAGHTON, P. J. 1988 *Phys. Rev.* A **37**, 3423.

SIMPSON, H. C., BEGGS, G. C. & DEANS, J. 1975 *Intl J. Heat Mass Transfer* **18**, 615.

TIRMIZI, S. H. & GILL, W. N. 1987 *J. Cryst. Growth* **85**, 488.

WILKINSON, J. 1955 *Q. J. Mech. Appl. Maths* **8**, 415.

XU, J. J. 1988 *Phys. Rev.* A **37**, 3087.